ION ACTIVITY IN QUASI-NEUTRAL CURRENT SHEETS AND DISCHARGE PLASMA IN CROSSED ELECTRIC AND MAGNETIC FIELDS

N.A. Strokin

Irkutsk National Research Technical University,
Irkutsk, Russia, strokin85@inbox.ru

Abstract. As part of a brief review, a classification is made and information is provided about four experimentally discovered plasma effects, where unexpected behavior of the ionic component appeared and for which there is

no unambiguous interpretation. 1. Ions with the highest energies for a quasi-neutral current sheet were recorded at the O-point (island) with the direction of their movement opposite to the electric field at the X-point. 2. In a self-sustaining discharge in crossed electric and magnetic fields (**E**×**B** discharge), a large number of ions (not the tails of the distribution function) with energies significantly exceeding the energies equivalent to the discharge voltage are generated. This occurs in a certain range of pressures of the plasma-forming gas and magnetic fields. 3. The discovered region of effective ionization — the "anode layer", with increasing pressure, moves abruptly from one plasma region to another, which is accompanied by a jump in the ion density up to 16 times. An increase in the mag-

netic field induction causes, on the contrary, the "anode layer" to jump in the opposite direction with the ion density decreasing 3–4 times. 4. Ion distribution functions in the **E**×**B** discharge contain isomagnetic density jumps with a relative amplitude from ∼30 to 80 % of the total current at the released energy. Taking into account the "anomalous" behavior of ions in the plasma of quasi-neutral current sheets and discharges in crossed electric and magnetic fields will provide further insight into the processes in space plasma, the physics of coronal heating, and the formation of the solar wind.

Keywords: ion acceleration, quasi-neutral current sheet, discharge plasma in crossed electric and magnetic fields.

INTRODUCTION

As the most energy-intensive part of plasma the ionic component is of particular interest to researchers. The processes implemented in space and laboratory plasma reveal effects associated with the unexpected behavior of ions. For instance, explosive processes in the Sun generate protons with energies exceeding $W \sim 100$ MeV. Information about this is obtained by recording the γ radiation of nuclear lines and through direct measurements of particle fluxes with spacecraft instruments [Aschwanden, 2019; Gopalswamy et al., 2021]. The γ-ray spectrum may be discontinuous in time, thereby indicating the presence of more than one source of high-energy protons or their additional acceleration [Kocharov et al., 2021]. In the standard flare model, the seed process of ion acceleration is the magnetic reconnection in a quasi-neutral current sheet (QNCS is a current sheet with a magnetic field component transverse to its plane) of a coronal loop with antiparallel magnetic field lines when the magnetic field topology changes [Priest, Forbes, 2000; Shibata, Magara, 2011; Aschwanden, 2022]. For solar flares, the "need" for zero points (places where electrons can accelerate in induced electric fields of bipolar sunspots) was first noted in [Giovanelli, 1946, 1948]. The energy gathered here by electrons exceeds the excitation potentials of atoms, which explains the observed solar plasma radiation flux during chromospheric flares. Dungey [1953] introduced the concept of X-points of a zero magnetic field and areas of

closed field lines — O-points (islands). In addition, the author examined the processes of discontinuity and reconnection of magnetic field lines when their total length and field energy decrease, and particles gain energy $W = e|\vec{u}||\vec{H}|l / c$ in an induced electric field $\vec{E} = -\vec{u} \times \vec{H} / c$, where u is the particle velocity; H is the magnetic field strength at a distance l from the zero point. Dungey [1953] also indicated that near the neutral point the magnetic field instability leads to the formation of discrete filaments, which allowed Sweet [1958] to show that at hydrostatic pressure $P_M > \lambda_3 H_0^2 / (4\pi)$ the maximum current density in the formed collisional layer $j_{max} > c\lambda_1 H_0 / (4\pi L)$, where H_0, L are the typical field strength and linear dimensions of the field region; λ_1, λ_3 are constants. Parker introduced the concept of reconnection and showed that the rate of dissipation of oppositely directed magnetic fields according to Sweet — stationary reconnection in the case of high but finite conductivity $\sigma \sim 10^{13}$ S at the characteristic solar scale $L = 10^9$ cm and density 10^{-21} g/cm^3 becomes much higher than the diffusion rate [Parker, 1957]. Such QNCS stability, termed as the tiring instability, develops if there is a conduction disturbance with a wavelength greater than the thickness of the sheet, and the time of resistive diffusion of the magnetic field in

the sheet $\tau_R = l^2 / (\mu\sigma) \gg \tau_A = l / V_A$, where τ_A is the Alfvén crossing time of QNCS, $2l$ is the QNCS thickness, $\gamma_m \approx \sqrt{\tau_R / \tau_A}$ is the maximum increment [Furth et al., 1963]. Higher reconnection rates are obtained by taking into account dissipation due to Hall movements and by considering kinetic effects [Aschwanden, 2019]. Another approach is the transition to high aspect ratios L/l and a turbulent medium [Loureiro et al., 2009; Uzdensky, Loureiro, 2016]. The turbulent external disturbance, which locally enhances the development of the tiring instability, is characterized by the turbulence power ε per unit area. The effective reconnection rate relative to the reconnection rate in the laminar case $\gamma_{eff} / \gamma_{SP} \sim \varepsilon^\alpha$, where $\alpha \approx$ 0.15÷0.25. QNCS fluctuates relative to its position, and secondary islands are formed in it — plasmoids growing in size. This instability was called plasmoid with $\gamma\tau_A \sim S^{1/4}$, where S is the Lundquist number. Uzdensky, Loureiro [2016] have shown that the plasmoid instability in the multi-island mode (Coppi mode) can develop during the formation of QNCS.

Energy dissipation at different rates under changes in plasma conductivity occurs when two islands merge [Biskamp, Welter, 1980] or during multiple reconnection [Potter et al., 2019]. When the islands merge, the vertical size of the structures corresponding to the X-line can significantly exceed the ion inertial length; therefore, ions and electrons of the preheated plasma inside the merging islands are heated impulsively with $\tau \sim 10\omega_{Hi}^{-1}$ (ω_{Hi} is the ion gyrofrequency) [Nakamura et al., 2023]. Formation of various plasmoids in a constantly elongated QNCS was recorded in a solar flare on July 19, 2012 [Lu et al., 2022]. Flows in the reconnection region and plasmoids are shown in EUV images (131 Å). X-ray measurements (1–8 Å — electron fluxes with an energy 6–100 keV) demonstrated sources of nonthermal radiation in the lower part of vertical

QNCS, presumably in a large plasmoid with trapped energetic electrons. In the radio range (drift velocities of 0.68, 1.22, and 1.96 MHz·s^{-1}), upward (~1035 km·s^{-1}) and downward (~640 km·s^{-1}) pulsating structures were observed. An unusual pair of oppositely drifting plasmoids had initial heights of $3.4\cdot10^5$ and $3.1\cdot10^5$ km. These structures are assumed to reflect the evolution of primary and secondary plasmoids, formed in QNCS, and cascading magnetic reconnection.

Crossed electric and magnetic fields are typical both for the solar atmosphere and for discharges in devices of terrestrial origin, such as plasma accelerators [Zhurin, 1999; Choueiri, 2001; Goebel, Katz, 2008; Abolmasov, 2012; Kaganovich et al., 2020], ion fluxes from which are used, for example, for correcting spacecraft orbits [Kim et al., 2007]. These are stationary plasma thrusters (SPTs) and thrusters with anode layer (TAL) [Zhurin et al., 1999; Choueiri, 2001; Kim et al., 2007; Goebel, Katz, 2008; Garrigues, Coche, 2011; Abolmasov, 2012; Kaganovich et al., 2020; Simmonds, Raitses, 2021], in which a stationary abnormal glow discharge burns in crossed electric and magnetic fields (**E**×**B** discharge).

In this paper, we present data from experiments in current and discharge plasma with magnetic and electric fields, which allowed us to detect considerable fluxes of abnormal charged particles — ions accelerated to energies exceeding the equilibrium ones. The purpose of this work is to call researchers' attention to common features of the objects under study: 1) the macroscopic nature of ion generation mechanisms; 2) most ions accelerate to high energies in areas of stationary or moving jumps in electrostatic potential, which are formed with parameters determined, among other things, by collective mechanisms of energy dissipation; 3) triggers of accelerating processes are certain forming configurations and strengths of electric and magnetic fields.
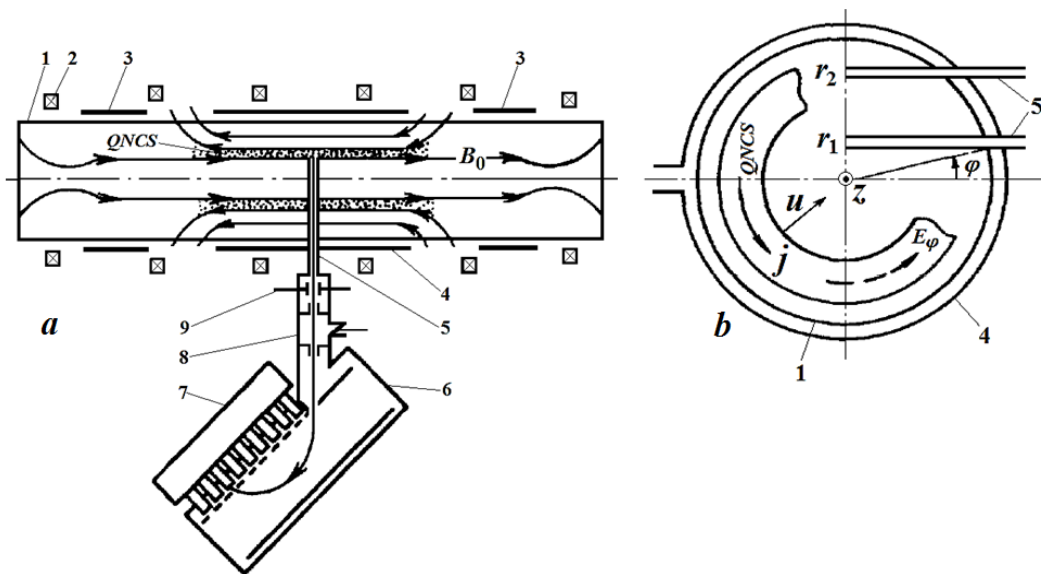

Figure 1. Scheme of θ-pinch type installation "UN-Fenix": top view (*a*), diametrical sectional view (*b*). 1 — quartz vacuum volume, 2 — Helmholtz coils, 3 — pre-ionization coils, 4 — shock coil, 5 — channels of extraction of neutrals, 6 — multichannel ion energy analyzer, 7 — PEM unit, 8 — stripping chamber, 9 — capacitor for cleaning up a beam of atoms from ions. Adapted from [Koshilev et al., 1977]

1. EXPERIMENTAL INSTALLATIONS

The results presented in this paper have been obtained in experiments carried out using two installations and their modifications. Chronologically, the first of them is a θ-pinch type installation "UN-Fenix" [Koshilev et al., 1977] (Figure 1), in which QNCS was created in a pre-created hydrogen plasma in a cylindrical quartz volume (1 m in length, 0.18 m in diameter) with the initial density $n_0 = 10^{18} \div 10^{20}$ m^{-3} and the initial electron and ion temperature $T_{0e} \approx T_{0i} \approx 1 \div 5$ eV. The quasistationary homogeneous magnetic field ($B_0 = 0.01 \div 0.1$ T; period $T_0 \approx 1$ ms) was directed along the axis of the system. The pre-created plasma at a length of 30 cm in the central region of the working volume was subject to impact by a cylindrical magnetic piston — the field B_1 in the form of an aperiodic pulse with a half-height duration of ~3.5 ms, which increases sinusoidally over the time $\Delta t \approx 450$ ns to $B_1 \approx 0.14$ T and directed toward the field B_0. A QNCS $\Delta \approx 2$ cm thick was formed which first moved toward the axis of the system and then stopped at some distance from it. Energy spectra were measured of ions moving relative to the QNCS plane in various directions — radial (see Figure 1, *a*), azimuthal (Figure 1, *b*), and along the QNCS.

The second installation is a one- or two-chamber plasma accelerator with anode layer [Bardakov et al., 2014; Strokin et al., 2019a], which is a source of a single or multicomponent ion flow (Figure 2). The radius of the central trajectory of the output window for ions in the TAL cathode $R = 90$ mm, the window width is 5–6 mm. An example of the distribution of the magnetic field radial component in the discharge gap of one-chamber TAL is given in Figure 2, *b*. Operating discharge voltages were set in the range $U_d = 300 \div 2000$ V. At given B, U_d, and plasma-forming gas (gases) pressure $P = 5 \cdot 10^{-5} \div 3 \cdot 10^{-4}$ torr, discharge currents $I_d \leq 300$ mA.

Figure 3 shows a scheme of the two-chamber TAL used in ion acceleration experiments. Anode-2 (position 2), made of non-magnetic steel, could be electrically isolated from cathode magnetic core (3). In this case, it was either supplied with an electric potential U_{A2}, or it could be under a floating potential U_{fl}. At the same time, TAL became two-chamber.
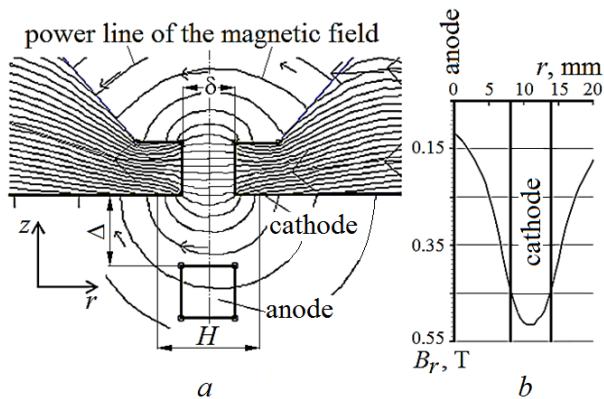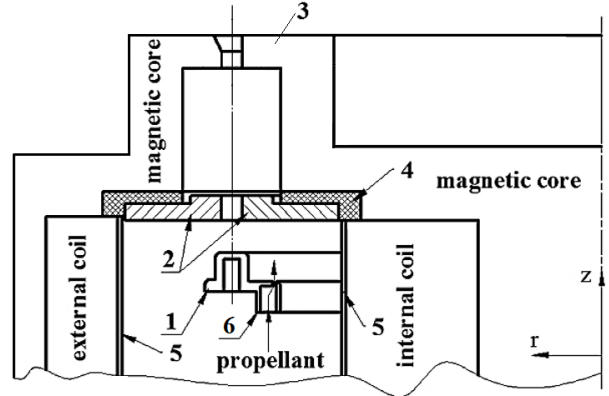

Figure 3. Scheme of two-chamber TAL: 1 — anode-1, 2 — anode-2, 3 — cathode magnetic core, 4 — insulator, 5 — screens, 6 — gas distributor

Discharge chamber in the anode-1 — anode-2 region is limited by metal screens 5, which were grounded or under floating potential. The anode-1 — anode-2 distance was 8 mm; the anode-2 — cathode, 30 mm. Plasma-forming gases are helium, nitrogen, and argon. In the anode-1—anode-2 interval, where the magnetic field radial component B_r was monotonously increasing, B_z did not exceed 13 % of B_r. The work was carried out at different values of magnetic induction, which was determined by the currents in internal and external TAL coils. The gas flow range was 0.1–0.8 mg/s; the TAL discharge pressure did not exceed $2 \cdot 10^{-4}$ torr. The plasma density in the near-field plume did not exceed $n = 10^{15}$ m^{-3}. The electron temperature T_e was 20–27 eV. The distributions of density, electron temperature, and plasma potential are inhomogeneous in radius and track the movement of the ion flow along the radius.

2. MEASUREMENT METHODS

Energy spectra of protons in QNCS were reconstructed from energy distributions of neutral charge-exchange particles with a process scheme: $\vec{H}^+ + H^0 \rightarrow \vec{H}^0 + H^+$, where an arrow indicates a fast particle. Neutral particles (hydrogen) carrying information about the energy spectrum of protons were transformed into protons on a gas target in stripping chamber 8 (see Figure 1) and were analyzed in an electrostatic field. In this work, 9- and 8-channel energy analyzers of neutral charge-exchange particles have been applied [Koshilev et al., 1977; Borzenko et al., 1978], which include a multichannel electrostatic ion analyzer: reflecting mirror 6 and recording system 7, which is a combination of ion-electronic converters — scintillators — photoelectronic multipliers. The time resolution of the 8-channel neutral particle energy analyzer was 4–160 ns. Ion energy distributions at the TAL outlet were measured by the ion energy analyzer with a retarding field (RFA) operating in coordination with a data control, acquisition, and pre-processing system [Bardakov et al., 2015]. The magnitude and time profile of the electrostatic potential in moving QNCS were estimated using double floating electric probes whose reference

Figure 2. Scheme of TAL's discharge gap (*a*); magnetic induction distributed along the discharge gap (*b*): δ≈6 mm, Δ≈10 mm, H≈14 mm — region of electronic emission from the cathode surface

electrode was in the initial (undisturbed) plasma. The second electrode looked like a plane perpendicular to the normal to QNCS. The potential distribution in the stationary plasma was measured by emission probes. The initial plasma density n_0 was monitored by a triple Langmuir probe. The electron temperature T_e was estimated from the volt-ampere characteristic of Langmuir probes.

3. RESULTS

3.1. Ion acceleration in a quasi-neutral current sheet

From 80 to 200 ns, magnetic islands are formed in QNCS moving toward the axis in plasma of the UN-Fenix installation approximately at a velocity V_A due to the development of a tiring instability. The typical magnetic field topology after the QNCS stopped ($t \geq 200$ ns) at a radius $r \approx 6$ cm is shown in Figure 4, *a*. There are two pronounced islands joined by common field lines and separated by an X-point. In the range $300 \leq t \leq 1200$ ns, the magnetic structure remains almost unchanged. The field B_1 at the plasma boundary, after reaching a maximum at $t_m \approx 450$ ns, slowly decreased in amplitude and by $t_1 \approx 1.5$ ms approached the level of the quasistationary field B_0 [Altyntsev et al., 1988, 1990]. At the same time, the outer boundary of the island shifted to the wall of the operating volume, and the closed magnetic configuration opened (Figure 4, *b*, *c*). The opening time is $(2 \div 3)t_A$, where t_A is the transit Alfvén time across the island.
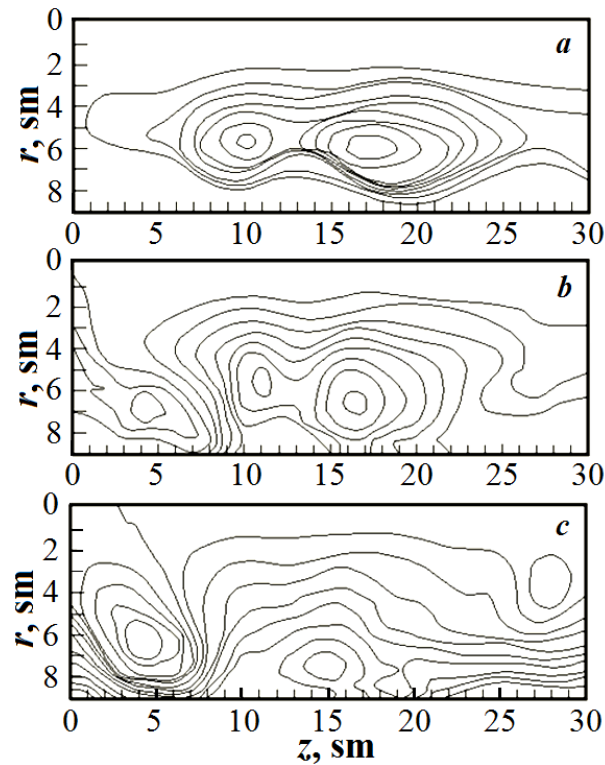

Figure 4. Magnetic flux isolines: $t=300$ (*a*), 1200 (*b*), 1600 (*c*) ns. The step of plotting the isolines is 1000 G·cm², $B_0=0.031$ T, $n_0=1.5 \cdot 10^{19}$ m⁻³, $z=0$ — wall. Adapted from [Altyntsev et al., 1988]

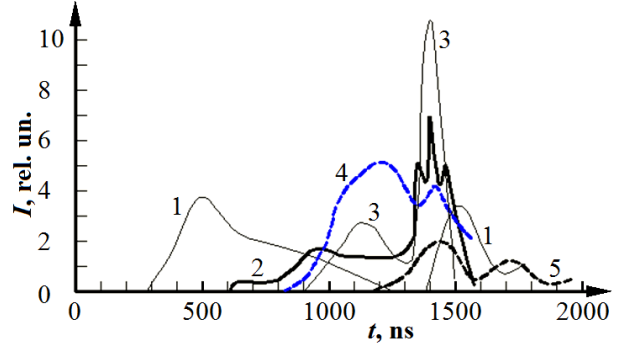*Figure 5.* Signals from ion energy analyzer collectors: 1 — 410, 2 — 778, 3 — 1165, 4 — 1461, 5 — 4697 eV; radial measurements (α=90°), z=18 cm. Adapted from [Altyntsev et al., 1990]
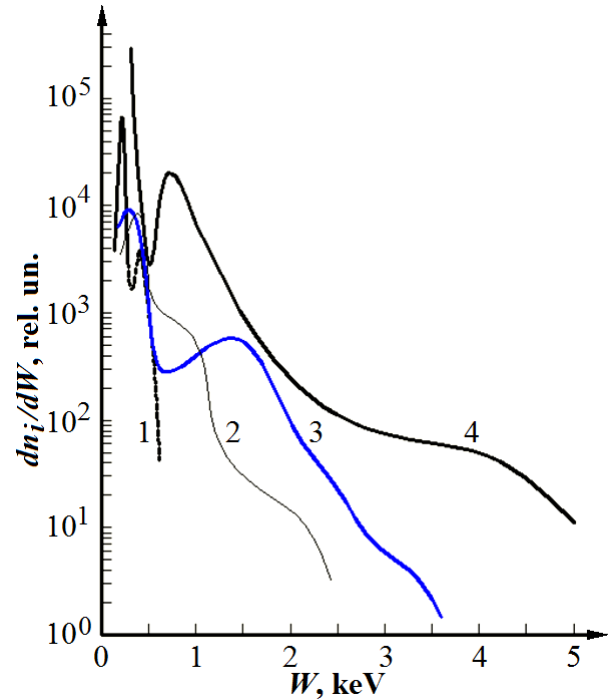

Figure 6. Ion energy distributions: 1 — t=140, 2 — t=700, 3 — t=1000, 4 — t=1400 ns. Adapted from [Altyntsev et al., 1990]

Signals from several detectors of the neutral charge-exchange particle energy analyzer with a particle output channel installed radially in front of a large island (z=18 cm) are exhibited in Figure 5. Ions with increasingly high energies were sequentially recorded (curves 1–5). When the magnetic structure was opened (rearranged) ($t \geq 1400$ ns), an intense burst of ion radiation was observed in the entire operating energy range of the analyzer. In this case, accelerated ions moved in the direction opposite to the electric field at the X-point.

The signals shown in Figure 5 were used to construct ion energy spectra (Figure 6) from which the rate of energy gain by protons $dW/dt=(2 \div 6) \cdot 10^9$ eV/s was calculated. Thus, under forced destruction of the islands of the "old" magnetic structure, ions gain energy, maximum of the energies recorded in QNCS, at a rapid rate.

3.2. Plasma in crossed E×B fields. Acceleration of ions to energies exceeding the energies equivalent to discharge voltage

The scheme of the two-chamber TAL used in this experiment is shown in Figure 3 [Bardakov et al., 2016, 2018]. Ion energy distribution functions were measured by a three-grid RFA at the TAL outlet. Ions abnormally accelerated to energies $W>eU_d$ have been detected. Examples of data when argon was the plasma-forming gas are given in Figure 7.

It was expected that the spectra shifted to high energies within the range determined by the discharge voltage. It is associated with the movement of ionization and acceleration zones in the anode — TAL cathode space (spectra 1 and 2). Nonetheless, with an increase in pressure above $P\approx9\cdot10^{-5}$ torr (spectra 3–5) the ion energy distribution function moved out of the boundary $W=eU_d=1100$ V (bold vertical line) through an unidentified plasma ion acceleration mechanism.

The most probable ion energy W_m as a function of magnetic field induction in TAL is plotted in Figure 8. It can be seen that there are no ions with $W_m>eU_d$ at $P=9\cdot10^{-5}$ torr for all magnetic fields of the operating range. When $P\geq1.2\cdot10^{-4}$ torr, super-accelerated ions appear at $B_{r1A}\geq2.7\cdot10^{-2}$ T. During induction at the anode $B_{r1A}\geq4.1\cdot10^{-2}$ T, the generation of ions with $W_m>eU_d$ is suppressed.
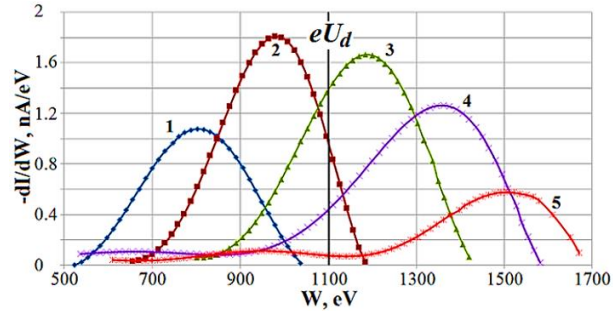

Figure 7. Evolution of argon ion energy distributions as pressure changes: 1 — $P=7\cdot10^{-5}$, 2 — $8\cdot10^{-5}$, 3 — $9\cdot10^{-5}$, 4 — $1\cdot10^{-4}$, 5 — $1.2\cdot10^{-4}$ torr; $U_d=1100$ V; magnetic field radial component at anode-1 $B_{r1A}\approx3.78\cdot10^{-2}$ T; anode-2 is under the floating potential $U_{A2}=U_{fl}$
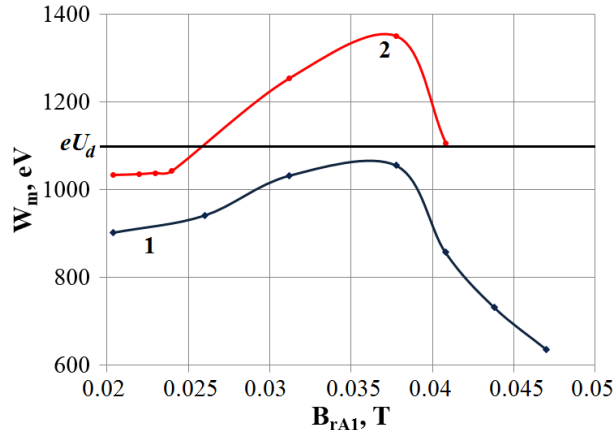

Figure 8. The most probable energy of argon ions as a function of magnetic field induction in the region of the first anode: curve 1 — $P=9\cdot10^{-5}$, 2 — $1.2\cdot10^{-4}$ torr; the horizontal line corresponds to eU_d

3.3. Plasma of E×B discharge. Jumps of the anode layer

In a self-sustaining **E×B** discharge, Strokin et al. [2019b] have found sharp changes in the ion energy distribution function, which are determined by the position of the anode layer (AL) in the anode—cathode gap of single-cascade TAL (see Figure 2). AL is understood here as a region bounded along the TAL axis in the interelectrode space, where effective ionization of neutrals occurs when they collide with electrons. AL jumps from the anode region to the cathode region were accompanied by an abrupt (up to 16 times) increase in ion density from 10^6 to $1.6\cdot10^7$ cm^{-3} (Figure 9, insert). The ion energy distributions in this case leapt toward low energies: the most probable energy decreased from $W_{m1}\approx756$ to $W_{m5}\approx328$ eV. At $P\approx1.2\cdot10^{-4}$ torr, electrons were heated to ~30 eV already in the cathode zone, which led to an exponential increase in the ionization cross-section of argon atoms during an electron impact, to the transfer of the ionization zone and acceleration to the cathode, and to an ion density jump.

3.4. Plasma of E×B discharge. Isomagnetic density jumps

Threshold effects were observed for ion density and energy distributions and under magnetic field induction changes in the discharge [Strokin et al., 2019b]. A 3–4-fold decrease in density was observed when the magnetic field radial component at the anode B_{rA} increases (and hence when the field at the cathode changes) by only ~ 2–9 percent — these are isomagnetic density jumps occurring at almost constant B_{rA}. In this case, the most probable ion energies also change abruptly to high values (Figure 10). When processing the RFA delay curves without averaging over their associated spectra, we can see a fine energy structure — spatially confined (the estimate gives an axial size of about tenths of a millimeter) stationary regions with a high longitudinal electric field strength — one or two isomagnetic potential jumps, which are generators of ion density jumps. On the spectra, this manifests itself in the form of bursts of the distribution function in narrow energy ranges. Isomagnetic jumps move up or down in energy with the spectrum as B_{rA} varies. The relative ion current amplitude in the bursts ranges from ~30 to 80 % of the total ion current at the released energy. Spectra with one isomagnetic jump are exemplified in Figure 11, *a*; panel *b* presents a portion of the spectrum with two high-amplitude isomagnetic jumps.

4. DISCUSSION AND CONCLUSIONS

Reconnection of magnetic field lines is a fundamental physical process and occurs in many astrophysical and laboratory plasma objects, in particular as an element of key energy release and a driver in a complex chain of events. For instance, in [Melrose, 1990; Drake et al., 2006; Kocharov et al., 2021] stochastic acceleration, diffusion, and drift acceleration at shock wave fronts,
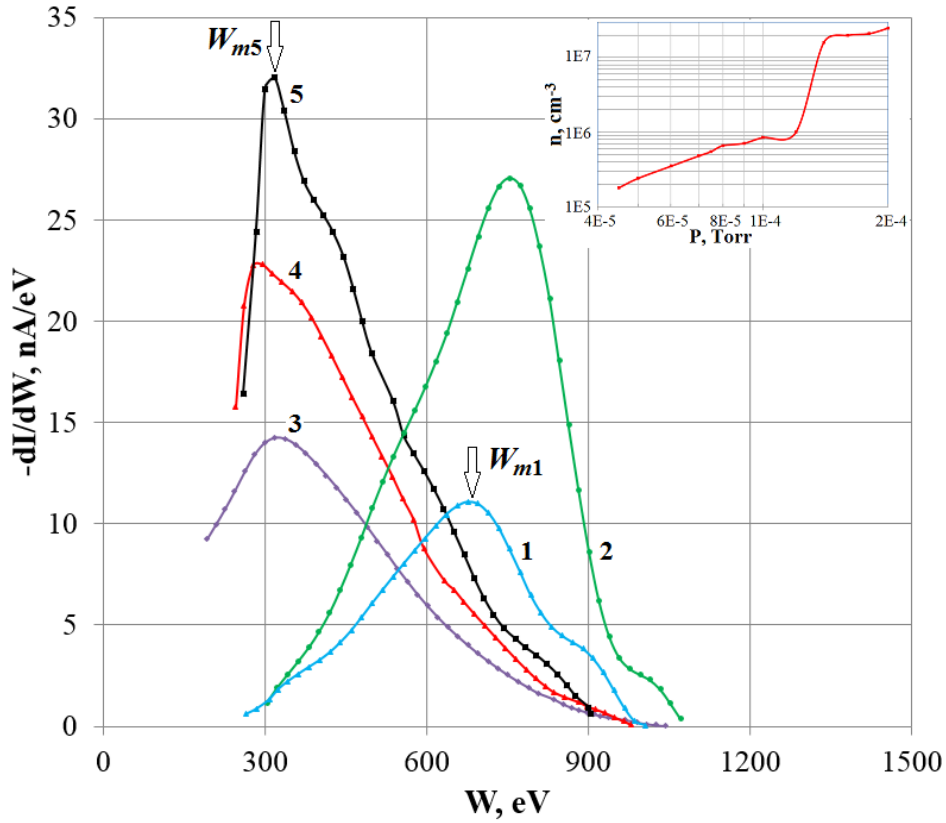
Figure 9. Abrupt change in ion energy and density jump (insert). Plasma-forming gas argon, $B_{rA}=0.097$ T, $U_d=1100$ V. Curve 1 — $P=7\cdot10^{-5}$, 2 — $1.2\cdot10^{-4}$, 3 — $1.4\cdot10^{-4}$, 4 — $1.8\cdot10^{-4}$, 5 — $2\cdot10^{-4}$ torr. The amplitudes of curves 1 and 2 are multiplied by 20
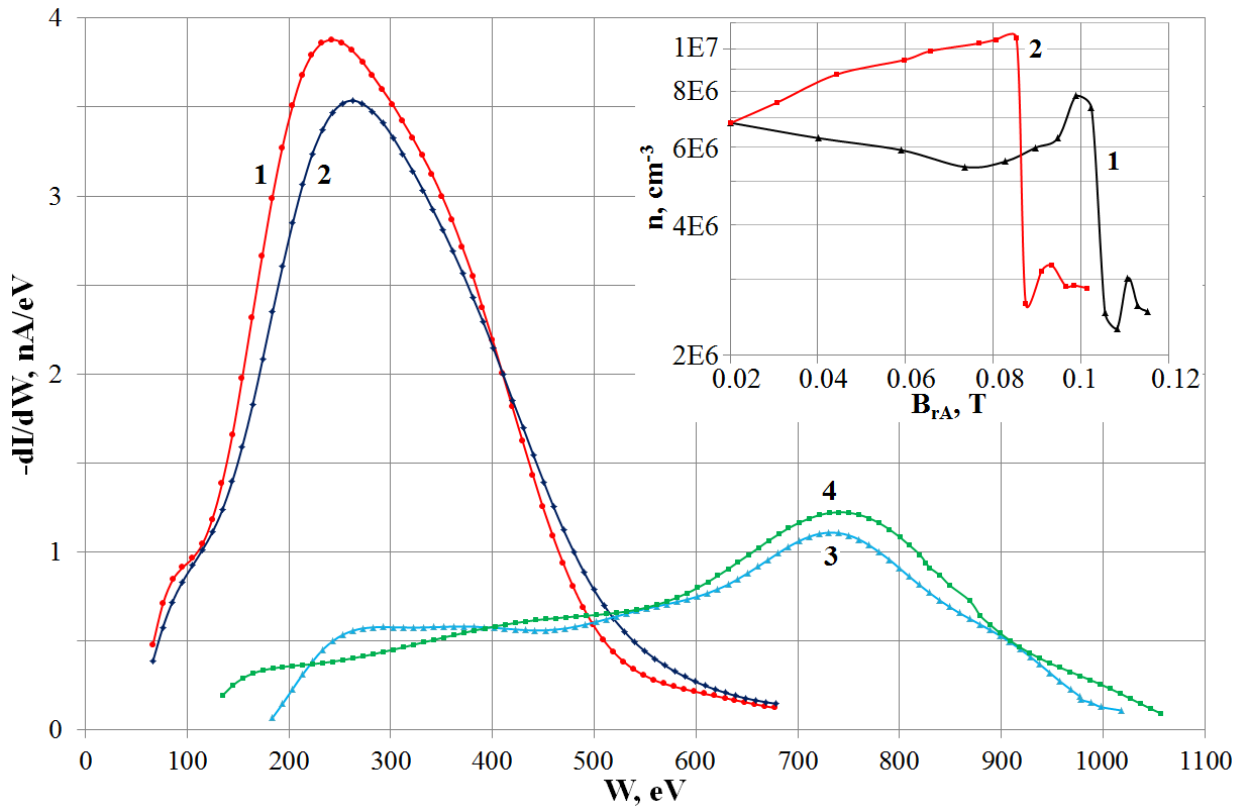

Figure 10. Energy spectra of ions at the TAL outlet. Plasma-forming gas argon, $U_d=1100$ V, $P=9\cdot10^{-5}$ torr. Curve 1 — $B_{rA}=0.02$, 2 — 0.04, 3 — 0.11, 4 — 0.115 T. The insert is the dependence of the ion density at the TAL outlet on magnetic field induction at the anode. Curve 1 — currents in two coils forming the field in TAL are the same $I_1=I_2$; curve 2, $I_1>I_2$
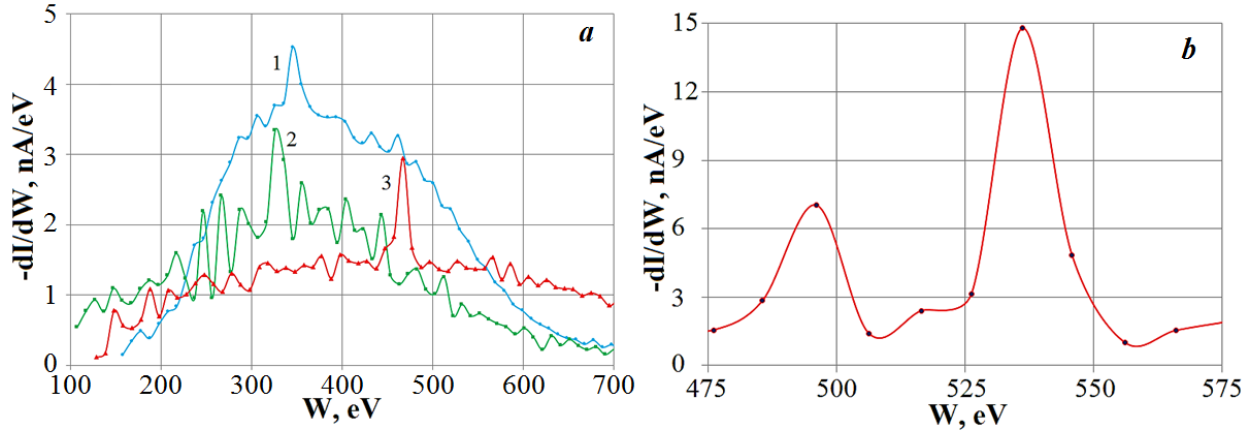
Figure 11. Examples of ion energy distributions at the TAL outlet: $P=9 \cdot 10^{-5}$ torr, $U_d=1100$ V; a — neon, curve 1 — $B_{rA} \approx 0.02$, 2 — $B_{rA} \approx 0.059$, 3 — $B_{rA} \approx 0.11$ T, $I_1=I_2$; b — argon, $B_{rA} \approx 0.09$ T; $I_1 \neq I_2$

generated by coronal mass ejections, resonant acceleration, acceleration in double layers, and acceleration during magnetic reconnection: collapse at the X-point and merging of islands (O-points), acceleration in collapsing magnetic islands and collapsing magnetic traps, were considered as accelerating mechanisms in solar flares.

In these works, there is no effective mechanism for accelerating ions in islands, including destructed ones, which was discovered in our laboratory experiments [Altyntsev et al., 1988, 1990]. Three-dimensional turbulent reconnection during the development of plasmoid instability is virtually postulated in the solar atmosphere [Drake et al., 2006; Shibata, Magara, 2011; Uzdensky, Loureiro, 2016; Potter et al., 2019; Lu, et al., 2022]. In the process of fragmentary magnetic reconnection, it seems possible that the magnetic field topology might exist in fractal QNCS when the magnetic field at the boundary of an island decreases, leading, as in [Altyntsev et al., 1988, 1990], to the destruction of the island and to the generation of accelerated ions in the direction opposite to the electric field at the X-point. Therefore, it makes sense to add and analyze another accelerating mechanism — generation of accelerated ions in the process of forced destruction of the islands of the QNCS old magnetic structure.

Note, by analogy with flares, that in the laboratory QNCS, along with the already mentioned one, several more ion acceleration mechanisms have been identified. Two regular acceleration mechanisms are manifested in the dynamic state: reflection from an electrostatic potential jump and a surfing acceleration mechanism. Energies of radially moving reflected ions $W_{ref} \leq W_{dir}=4 MU^{2/2}$, where U is the QNCS velocity; at a surfing acceleration $W_s \leq 80 \, W_{dir}$ for the azimuthal motion. The energy of ions propagating along the QNCS is determined by the ambipolar potential jump at the boundary of cold plasma outside the sheet and QNCS hot plasma, $W_{max} \leq 2$ keV [Altyntsev et al., 1988, 1990]. The magnetic field effect on the ion energy gain was also determined in fragments for the plasma diode [Shibata, Magara, 2011], in which W_m of magnesium ions decreased by 25 % as the longitudinal magnetic field increased from 0 to $1.7 \cdot 10^{-2}$ T. Having experimental quantitative evidence of the effectiveness of ion acceleration

in the reflection from an electrostatic potential jump in moving QNCS and the acceleration of ions trapped by the potential jump moving across the magnetic field along the current sheet, we can more confidently refer to them as major causes of the generation of fast ions.

For future research on discharges in crossed electric and magnetic fields, it is necessary to find a mechanism of charge separation in the TAL discharge gap and coronal plasma — the condition for the formation of a virtual anode whose potential jump will exceed the discharge voltage. In this case, the results obtained by Bardakov et al. [2016] will become clear.

The studies [Strokin et al., 2019a, b] have supplemented the list of phenomena and processes characterizing the abnormal self-sustained **E**×**B** discharge. Transformation has been detected in the ion distribution function, density, and potential with a change in the plasma-forming gas pressure — jumps from high to low energies. When magnetic field induction increased, reverse transfers were observed — from low to high energies. The ion energy distribution functions, potential, and electric field, as it turned out, have a complex fine structure in the form of isomagnetic jumps. Causes of such rearrangements should have a threshold dependence on the local density and/or energy of the electrons providing ionization of neutrals in the discharge region where the rearrangement takes place. An electron-cyclotron drift instability [Cavalier et al., 2013] may be a possible candidate for heating electrons during several inverse increments $\gamma^{-1} \approx \omega_{LH}^{-1}$ (ω_{LH} is the lower hybrid frequency) to an energy exceeding the ionization potential. Unstable modes of non-local gradient-drift instabilities of **E**×**B** discharges form zones with a high axial potential gradient, which can be called isomagnetic jumps [Romadanov et al., 2016]. They can be considered as causes of abrupt changes in the dependences $n=f(B)$ and in the ion energy distribution function. For plasma of the solar atmosphere, a change in the magnetic field strength and topology is a typical state that cannot but cause its associated threshold changes in the energy of charged particles and plasma density. The results obtained in **E**×**B** discharge plasma give some confidence in setting objectives of modeling similar processes in coronal and chromospheric plasma.

In this paper, through a thematic analysis, plasma effects, observed for the first time in experiments carried out by scientific teams assisted by the author, have been selected and summarized. In these effects, effective acceleration of the ionic plasma component was recorded. Taking into account the abnormal behavior of ions in plasma of quasi-neutral current sheets and discharges in crossed electric and magnetic fields is assumed to provide further insight into the processes in cosmic plasma, physics of coronal heating, and the formation of the solar wind. The necessity and possibility of this are assured by the increasing ability to directly measure small-scale events in the solar atmosphere with spacecraft, the most remarkable of which nowadays is the Parker Solar Probe [Kasper et al., 2021].

REFERENCES

Abolmasov S.N. Physics and engineering of crossed-field discharge devices. *Plasma Sources Science and Technology*. 2012, vol. 21, no. 035006. DOI: 10.1088/0963-0252/21/3/035006.

Altyntsev A.T., Lebedev N.V., Strokin N.A. Acceleration of ions in a current sheet with magnetic islands. *Phys. Lett. A*. 1988, vol. 129, no. 5-6, pp. 326–328. DOI: 10.1016/0375-9601(88)90342-8.

Altyntsev A.T., Lebedev N.V., Strokin N.A. Ion acceleration in a quasi-neutral current sheet. *Planet. Space Sci.* 1990, vol. 38, no. 6, pp. 751–763. DOI: 10.1016/0032-0633(90)90034-n.

Aschwanden M.J. New Millennium Solar Physics. Springer Cham: Switzerland AG. 2019. P. 714. DOI: 10.1007/978-3-030-13956-8.

Aschwanden M.J. Particle acceleration and kinematics in solar flares. A Synthesis of Recent Observations and Theoretical Concepts. *Space Sci. Rev.* 2022, vol. 101, pp. 1–227. DOI: 10.1023/A:1019712124366.

Bardakov V.M., Ivanov S.D., Strokin N.A. Advances and problems in plasma-optical mass-separation. *Phys. Plasmas*. 2014, vol. 21, no. 033505. DOI: 10.1063/1.4846898.

Bardakov V.M., Ivanov S.D., Kazantsev A.V., Strokin N.A. A noise-immune hardware-software complex for data acquisition and preprocessing in experiments on plasma-optical mass separation. *Instruments and Experimental Techniques*. 2015, vol. 58, no. 3, pp. 359–363. DOI: 10.1134/S0020441215030045.

Bardakov V., Ivanov S., Kazantsev A., Strokin N., Stupin A. "Super-acceleration" of ions in a stationary plasma discharge. *Phys. Lett. A*. 2016, vol. 380, no. 42, pp. 3497–3499. DOI: 10.1016/j.physleta.2016.06.028.

Bardakov V.M., Ivanov S.D., Kazantsev A.V., Strokin N.A., Stupin A.N., Jiang B., Wang Z. Anomalous acceleration of ions in a plasma accelerator with an anodic layer. *Plasma Sci. Technol*. 2018, vol. 20, no. 035501. DOI: 10.1088/2058-6272/aa97cc.

Biskamp D., Welter H. Coalescence of Magnetic Islands. *Phys. Rev. Lett*. 1980, vol. 44, no. 16-21, pp. 1069–1072. DOI: 10.1103/PhysRevLett.44.1069.

Borzenko V.P., Koshilev N.A., Parfenov O.G., Strokin N.A. Multichannel charge-exchange energy analyzer with high time resolution. *Technical Physics*. 1978, vol. 48, no. 6, pp. 1174–1177. (In Russian).

Cavalier J., Lemoine N., Bonhomme G., Tsikata S., Honore C., Gresillon D. Hall thruster plasma fluctuations identified as the *E×B* electron drift instability: Modeling and fitting on experimental data. *Phys. Plasmas*. 2013, vol. 20, no. 082107. DOI: 10.1063/1.4817743.

Choueiri E.Y. Fundamental difference between the two Hall thruster variants. *Phys. Plasmas*. 2001, vol. 8, no. 8, pp. 5025–5033. DOI: 10.1063/1.1409344.

Drake J.F., Swisdak M., Che H., Shay M.A. Electron acceleration from contracting magnetic islands during reconnection. *Nature*. 2006, vol. 443, no. 11, pp. 553–556. DOI: 10.1038/nature05116.

Dungey J.W. Conditions for the occurrence of electrical discharges in astrophysical systems. *The London, Edinburgh and Dublin Philosophical Magazine and Journal of Science*: Ser. 7. 1953, vol. 44, no. 354, pp. 725–738. DOI: 10.1080/14786440708521050.

Furth H.P., Killeen J., Rosenbluth M.N. Finite-resistivity instabilities of a sheet pinch. *Physics of Fluids*. 1963, vol. 6, no. 4, pp. 459–484. DOI: 10.1063/1.1706761.

Garrigues L., Coche P. Electric propulsion: comparisons between different concepts. *Plasma Physics and Controlled Fusion*. 2011, vol. 53, no. 124011. DOI: 10.1088/0741-3335/53/12/124011.

Giovanelli R.G. A theory of chromospheric flares. *Nature*. 1946, no. 4003, pp. 81–82. DOI: 10.1038/158081a0.

Giovanelli R.G. Chromospheric flares. *Monthly Notices of the Royal Astronomical Society*. 1948, vol. 108, no. 2, pp. 163–176. DOI: 10.1093/mnras/108.2.163.

Goebel D.M., Katz I. *Fundamentals of Electric Propulsion: Ion and Hall Thrusters*. John Wiley & Sons, Hoboken, New Jersey, 2008, p. 486. DOI: 10.1002/9780470436448.

Gopalswamy N., Yashiro S., Mäkelä P., Xie H., Akiyama S. The Common Origin of High-energy Protons in Solar Energetic Particle Events and Sustained Gamma-Ray Emission from the Sun. *Astrophys. J.* 2021, vol. 915, no. 82, pp. 1–9. DOI: 10.3847/1538-4357/ac004f.

Kaganovich I.D., Smolyakov A., Raitses Y., Ahedo E., Mikellides I.G., Jorns B., Taccogna F., Gueroult R., et al. Physics of *E×B* discharges relevant to plasma propulsion and similar technologies. *Phys. Plasmas*. 2020, vol. 27, no. 120601. DOI: 10.1063/5.0010135.

Kasper J.C., Klein K.G., Lichko E., Huang Jia, Chen C.H.K., Badman S.T., Bonnell J., Whittlesey P.L., et al. Parker Solar Probe Enters the Magnetically Dominated Solar Corona. *Phys. Rev. Lett.* 2021, vol. 127, no. 255101. DOI: 10.1103/PhysRevLett.127.255101.

Kim V., Kozubsky K.N., Murashko V.M., Semenkin A.V. History of the Hall Thrusters Development in USSR. *Proceedings of the 30th International Electric Propulsion Conference IEPC-2007-142, Florence, Italy, September 17–20, 2007.*.

Kocharov L., Omodei N., Mishev A., Pesce-Rollins M., Longo F., Yu S., Gary D.E., Vainio R., Usoskin I. Multiple Sources of Solar High-energy Proton. *Astrophys. J.* 2021, vol. 915, no. 12, pp. 1–9.

Koshilev N.A., Masalov V.L., Strokin N.A., Shishko A.A. Measurements of the ion energy spectrum in a collisionless neutral current sheet. *Sov. Phys. JETP*. 1977, vol. 45, no. 6, pp. 1108–1113.

Loureiro N.F., Uzdensky D.A., Schekochihin A.A., Cowley S.C., Yousef T.A. Turbulent magnetic reconnection in two dimensions. *Monthly Notices of the Royal Astronomical Society*. 2009, vol. 399, no. 1, pp. 146–150. DOI: 10.1111/j.1745-3933.2009.00742.x.

Lu L., Li F., Warmuth A., Veronig A.M., Huang J., Liu S., Gan W., Ning Z., Ying B., Gao G. Observational signatures of tearing instability in the current sheet of a solar flare. *Astrophys. J. Lett.* 2022, vol. 924, no. L7. DOI: 10.3847/2041-8213/ac42c6.

Melrose D.B. Particle Acceleration Processes in the Solar Corona. *Australian Journal of Physics*. 1990, vol. 43, no. 6, pp. 703–754. DOI: 10.1071/PH900703.

Nakamura T.K.M., The W.-L., Zenitani S., Umeda T., Oka M., Hasegawa H., Veronig A.M., Nakamura R. Spatial and time scaling of coalescing multiple magnetic islands. *Phys. Plasmas*. 2023, vol. 30, no. 022902. DOI: 10.1063/5.0127107.

Parker E.N. Sweet's mechanism for merging magnetic fields in conducting fluids. *JGR*. 1957, vol. 62, no. 4, pp. 509–520. DOI: 10.1029/JZ062i004p00509.

Potter M.A., Browning P.K., Gordovskyy M. Forced magnetic reconnection and plasmoid coalescence I. Magnetohydrodynamic simulations. *Astron. Astrophys*. 2019, vol. 623, no. A15. DOI: 10.1051/0004-6361/201833565.

Priest E., Forbes T. Magnetic reconnection. MHD theory and applications. Cambridge University Press: Cambridge. *Great Britain*, 2000, p. 600. DOI: 10.1017/CBO9780511525087.

Romadanov I., Smolyakov A., Raitses Y., Kaganovich I., Tian T., Ryzhkov S. Structure of nonlocal gradient-drift instabilities in Hall *E×B* discharges. *Phys. Plasmas*. 2016, vol. 23, no. 122111. DOI: 10.1063/1.4971816.

Shibata K., Magara T. Solar Flares: Magnetohydrodynamic Processes. *Living Rev. Solar Phys*. 2011, vol. 8, no. 6, p. 99. DOI: 10.12942/lrsp-2011-6.

Simmonds J., Raitses Y. Ion acceleration in a wall-less Hall thruster. *J. Appl. Phys*. 2021, vol. 130, no. 093302. DOI: 10.1063/5.0062607.

Strokin N.A., Bardakov V.M. Development of Idea of Plasma-Optical Mass Separation. *Plasma Physics Reports*. 2019a, vol. 45, No. 1, pp. 46-56. DOI: 10.1134/S1063780X19010148.

Strokin N.A., Kazantsev A.V., Bardakov V.M., Nguyen T.T., Kuzmina A.S. Jumping the anode layer in the zone of the *E×B* discharge. *Phys. Plasmas*. 2019b, vol. 26, no. 073501. DOI: 10.1063/1.5093778.

Sweet P.A. The neutral point theory of solar flares. Electromagnetic Phenomena in Cosmical Physics. *Proceedings of the International Astronomical Union*. 1958, vol. 6, pp. 123–134. DOI: 10.1017/S0074180900237704.

Uzdensky D.A., Loureiro N.F. Magnetic Reconnection Onset via Disruption of a Forming Current Sheet by the Tearing Instability. *Phys. Rev. Lett*. 2016, vol. 116, no. 105003. DOI: 10.1103/PhysRevLett.116.105003.

Zhurin V.V., Kaufman H.R., Robinson R.S. Physics of closed drift thrusters. *Plasma Sources Sci. Technol*. 1999, vol. 8, no. R1-R20. DOI: 10.1088/0963-0252/8/1/021.

How to cite this article
Strokin N.A. Ion activity in quasi-neutral current sheets and discharge plasma in crossed electric and magnetic fields. *Solar-Terrestrial Physics*. 2024. Vol. 10. Iss. 1. P. 10–18. DOI: 10.12737/stp-101202402.